Laser-induced torques in metallic ferromagnets

Frank Freimuth,* Stefan Blügel, and Yuriy Mokrousov
Peter Grünberg Institut and Institute for Advanced Simulation, Forschungszentrum Jülich and JARA, 52425 Jülich, Germany
(Received 8 August 2016; published 24 October 2016)

We study laser-induced torques in bcc Fe, hcp Co, and $L1_0$ FePt based on first-principles electronic structure calculations and the Keldysh nonequilibrium formalism. We find that the torques have two contributions, one from the inverse Faraday effect (IFE) and one from the optical spin-transfer torque (OSTT). Depending on the ferromagnet at hand and on the quasiparticle broadening the two contributions may be of similar magnitude, or one contribution may dominate over the other. Additionally, we determine the nonequilibrium spin polarization in order to investigate its relation to the torque. We find the torques and the perpendicular component of the nonequilibrium spin polarization to be odd in the helicity of the laser light, while the spin polarization that is induced parallel to the magnetization is helicity independent. The parallel component of the nonequilibrium spin polarization is orders of magnitude larger than the perpendicular component. In the case of hcp Co we find good agreement between the calculated laser-induced torque and a recent experiment.

DOI: 10.1103/PhysRevB.94.144432

I. INTRODUCTION

Several mechanisms induce torques on the magnetization in magnetically ordered materials when laser pulses are applied [1]. When circularly polarized light is used, an effective magnetic field parallel to the light wave vector acts on the magnetization due to the inverse Faraday effect (IFE) [2] [Fig. 1(a)]. The IFE is thought to play a crucial role in the laser-induced magnetization reversal in ferromagnetic thin films [3,4]. Additionally, there is a light-induced effective magnetic field perpendicular to both the magnetization and the light wave vector, which leads to the optical spin transfer torque (OSTT) [5] [Fig. 1(b)]. Besides these nonthermal effects, the laser-induced heating can also generate torques due to heat-induced modifications of the magnetic anisotropy fields [6]. Furthermore, laser pulses excite superdiffusive spin currents in magnetic heterostructures [7–10], which mediate spin-transfer torques when they flow from one magnetic layer into another [11]. Finally, the laser-induced heating drives spin currents due to the spin-dependent Seebeck effect, which leads to thermal spin-transfer torques in metallic spin valves [12].

In the following we will consider only the effective magnetic fields, torques, and nonequilibrium spin densities related to the IFE and OSTT. In ferromagnets the light-induced nonequilibrium spin density can generally exhibit a component parallel to the equilibrium magnetization as well as a perpendicular one. The perpendicular component exerts a torque on the magnetization and tilts it. This laser-induced torque has been investigated in metallic ferromagnets in recent experiments [13,14]: In Co a 50-fs laser pulse with a fluence of 1 mJ cm^{-2} induces an effective magnetic field whose perpendicular component has been estimated at 0.2 T. One experiment [13] was interpreted in terms of an initial out-of-plane tilting of the magnetization due to an out-of-plane torque [Fig. 1(b)], while the second experiment [14] was interpreted in terms of an initial in-plane tilting due to an in-plane torque [see Fig. 1(a)]. The out-of-plane tilting has been ascribed to the OSTT, and the in-plane tilting is expected from the IFE. Both experiments find that the magnetization is only tilted when circularly polarized light is used and that the effect changes sign when the helicity of the light is reversed. In both experiments the Co layer is sufficiently thick (10 nm) to assume that the laser-induced effective magnetic fields responsible for the magnetization tilting can be modeled theoretically based on the bulk electronic structure of Co, neglecting the Co/Pt interface. In one experiment [13] the Pt capping layer mainly serves to prevent oxidation of the Co layer. In the second experiment [14] the inverse spin-orbit torque (ISOT) [15] due to the structural inversion asymmetry at the Co/Pt interface is exploited to convert the magnetization tilting into an interfacial photocurrent.

On the theory side, for the special case of the light-propagation direction parallel to the magnetization, light-induced effective magnetic fields parallel to the magnetization have been studied in transition-metal ferromagnets [16] with *ab initio* methods as well as in the ferromagnetic Rashba model [17]. Both theoretical works find that not only circularly polarized light but also linearly polarized light induce effective magnetic fields parallel to the magnetization. Moreover, it was found that the light-induced spin polarization parallel to the magnetization is almost helicity independent in Fe, Co, and Ni [16]. Since, in contrast, the light-induced torques observed experimentally are odd in the helicity [14], it seems that effective magnetic fields perpendicular to the magnetization direction depend differently on the light helicity than the parallel component in these metallic ferromagnets.

In this work we use *ab initio* density functional theory in order to study all components of the light-induced nonequilibrium spin density and of the resulting torques and effective magnetic fields in Fe, Co, and FePt. This allows us to answer the two questions raised above: (i) Is the laser-induced torque on the magnetization in Fig. 1 pointing in the in-plane or out-of-plane direction? (ii) How do the parallel and perpendicular components of the light-induced effective magnetic field differ regarding their size and their dependence on the light polarization?

This paper is structured as follows: In Sec. II we describe our computational approach, which uses the Keldysh nonequilibrium formalism to obtain the response in second order to

*Corresponding author: f.freimuth@fz-juelich.de

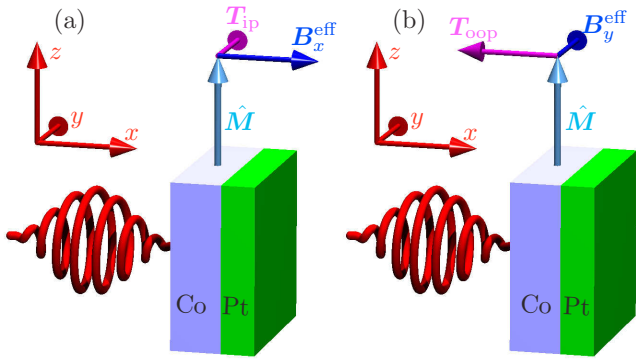

FIG. 1. A circularly polarized light pulse propagates in the x direction and hits a Co/Pt bilayer. The magnetization direction $\hat{\boldsymbol{M}}$ is along the z axis. The laser-induced torque $\boldsymbol{T}$ has two components: (a) The in-plane component $\boldsymbol{T}_{\rm ip}$ can be attributed to an effective magnetic field $\boldsymbol{B}_x^{\rm eff}$ in the x direction. $\boldsymbol{T}_{\rm ip}$ leads to an initial in-plane tilt of $\hat{\boldsymbol{M}}$. (b) The out-of-plane component $\boldsymbol{T}_{\rm oop}$ can be attributed to the y component $\boldsymbol{B}_y^{\rm eff}$ of a laser-induced effective magnetic field and leads to an initial out-of-plane tilt of $\hat{\boldsymbol{M}}$.

the electric field of the laser. Details of the derivation and of the numerical implementation are given in Appendix A and Appendix B, respectively. Before presenting our results in Sec. III we first describe the computational parameters used in the calculations in Sec. III A. In Sec. III B we discuss the effective magnetic fields that give rise to the laser-induced torques, and in Sec. III C we investigate the laser-induced nonequilibrium spin density. We conclude with a summary in Sec. IV.

II. COMPUTATIONAL METHOD

We use Kohn-Sham density functional theory to describe interacting many-electron systems by the effective single-particle Hamiltonian

$$H(\boldsymbol{r}) = H_0(\boldsymbol{r}) - \boldsymbol{m}\cdot\hat{\boldsymbol{M}}\Omega^{\rm xc}(\boldsymbol{r}), \tag{1}$$

where H_0 contains kinetic energy, scalar potential, and spin-orbit interaction (SOI), $\boldsymbol{m} = -\mu_{\rm B}\boldsymbol{\sigma}$ is the spin magnetic moment operator, $\mu_{\rm B}$ is the Bohr magneton, $\boldsymbol{\sigma} = (\sigma_x,\sigma_y,\sigma_z)^{\rm T}$ is the vector of Pauli spin matrices, $\hat{\boldsymbol{M}}$ is a normalized vector parallel to the magnetization, $\Omega^{\rm xc}(\boldsymbol{r}) = \frac{1}{2\mu_{\rm B}}[V^{\rm eff}_{\rm minority}(\boldsymbol{r}) - V^{\rm eff}_{\rm majority}(\boldsymbol{r})]$ is the exchange field, and $V^{\rm eff}_{\rm minority}(\boldsymbol{r})$ and $V^{\rm eff}_{\rm majority}(\boldsymbol{r})$ are the effective potentials of minority and majority electrons, respectively.

The interaction with the laser field is described by the perturbation to the Hamiltonian

$$\delta H(t) = e\boldsymbol{v}\cdot\boldsymbol{A}(t), \tag{2}$$

where e is the elementary positive charge, $\boldsymbol{v}$ is the velocity operator, and

$$\boldsymbol{A}(t) = {\rm Re}\left[\frac{E_0\boldsymbol{\epsilon}e^{-i\omega t}}{i\omega}\right] \tag{3}$$

is the vector potential. The corresponding electric field of the laser is

$$\boldsymbol{E}(t) = -\frac{\partial\boldsymbol{A}(t)}{\partial t} = {\rm Re}[E_0\boldsymbol{\epsilon}e^{-i\omega t}], \tag{4}$$

where $\boldsymbol{\epsilon}$ is the light-polarization vector and E_0 is the amplitude of the electric field. We assume that E_0 is real valued. However, $\boldsymbol{\epsilon}$ may be complex. For example, to describe left-circularly and right-circularly polarized light propagating in the x direction we use $\boldsymbol{\epsilon} = (0,1,i)/\sqrt{2}$ and $\boldsymbol{\epsilon} = (0,1,-i)/\sqrt{2}$, respectively.

The laser-induced change of spin polarization is given by [17–20]

$$\delta\boldsymbol{S} = \int d^3r\,\delta\boldsymbol{s}(\boldsymbol{r}) = \frac{\hbar}{2i}{\rm Tr}[\boldsymbol{\sigma}G^<], \tag{5}$$

where $G^<$ is the lesser Green's function. $\delta\boldsymbol{S}$ is the integral of the nonequilibrium spin density $\delta\boldsymbol{s}(\boldsymbol{r})$ over the simulation volume, i.e., the change of the total electron spin in the simulation volume, when $\hat{\boldsymbol{M}}$ in Eq. (1) is kept fixed. The torque on the magnetization due to the nonequilibrium spin density is given by [15,21–23]

$$\boldsymbol{T} = \frac{2\mu_{\rm B}}{\hbar}\int d^3r\,\Omega^{\rm xc}(\boldsymbol{r})\delta\boldsymbol{s}(\boldsymbol{r})\times\hat{\boldsymbol{M}}. \tag{6}$$

Since the nonequilibrium spin density $\delta\boldsymbol{s}(\boldsymbol{r})$ and the exchange field $\Omega^{\rm xc}(\boldsymbol{r})$ vary strongly on the atomic scale, it is generally not possible to calculate $\boldsymbol{T}$ exactly from $\delta\boldsymbol{S}$. Therefore, we calculate the torque from

$$\boldsymbol{T} = i{\rm Tr}[\boldsymbol{\mathcal{T}}G^<], \tag{7}$$

where $\boldsymbol{\mathcal{T}}(\boldsymbol{r}) = \boldsymbol{m}\times\hat{\boldsymbol{M}}\Omega^{\rm xc}(\boldsymbol{r})$ is the torque operator [15,23–26]. It is clear that the laser-induced nonequilibrium magnetization in paramagnets and diamagnets consists of both spin and orbital contributions. Consequently, a recent *ab initio* study on the IFE considered both spin and orbital parts of the laser-induced nonequilibrium magnetization [16]. However, in the present work we are mostly interested in the laser-induced torques on the magnetization in ferromagnets, which are determined by the nonequilibrium spin density according to Eq. (6). While the laser-induced orbital magnetization corresponds to orbital currents, which lead to magnetic fields according to the Maxwell equations, the resulting torques are negligible in comparison to the torques described by Eq. (6). We therefore do not consider the laser-induced orbital magnetization in this work.

In systems with broken inversion symmetry, $\boldsymbol{T}$ contains a contribution that is first order in $\boldsymbol{E}(t)$, the so-called spin-orbit torque (SOT) [15,23,24,26–28]. However, this first-order contribution oscillates with frequency ω. Since the light frequency ω is much higher than the ferromagnetic resonance frequency, this oscillating contribution will not induce significant magnetization dynamics. Therefore, we consider the dc part in the response to a continuous laser field. The contribution to $\boldsymbol{T}$ that is second order in $\boldsymbol{E}(t)$ contains such static terms. They can arise, for example, from the time-independent part $E_0^2{\rm Re}[\epsilon_i\epsilon_j^*]/2$ in

$$E_i(t)E_j(t) = \frac{E_0^2}{4}[\epsilon_i\epsilon_j^* + \epsilon_i^*\epsilon_j + \epsilon_i\epsilon_j e^{-2i\omega t} + \epsilon_i^*\epsilon_j^* e^{2i\omega t}]. \tag{8}$$

The dc correction of $G^<$ proportional to E_0^2 can be conveniently derived within the Keldysh nonequilibrium formalism. Details of the derivation are given in Appendix A. The resulting torque is given by the expression

$$T_i = \frac{a_0^3 I}{c}\left(\frac{\mathcal{E}_\mathrm{H}}{\hbar\omega}\right)^2 \mathrm{Im}\sum_{jk}\epsilon_j\epsilon_k^*\chi_{ijk}, \tag{9}$$

where c is the velocity of light, $a_0 = 4\pi\epsilon_0\hbar^2/(me^2)$ is Bohr's radius, $I = \epsilon_0 c E_0^2/2$ is the intensity of light, ϵ_0 is the vacuum permittivity, and $\mathcal{E}_\mathrm{H} = e^2/(4\pi\epsilon_0 a_0)$ is the Hartree energy. The tensor χ_{ijk} is given by

$$\begin{aligned}\chi_{ijk} = \frac{2}{\mathcal{N}\hbar a_0^2\mathcal{E}_\mathrm{H}}\sum_{\boldsymbol{k}}\int d\mathcal{E}\\ \times \mathrm{Tr}\big[&f(\mathcal{E})\mathcal{T}_i G^\mathrm{R}_{\boldsymbol{k}}(\mathcal{E})v_j G^\mathrm{R}_{\boldsymbol{k}}(\mathcal{E}-\hbar\omega)v_k G^\mathrm{R}_{\boldsymbol{k}}(\mathcal{E})\\ -&f(\mathcal{E})\mathcal{T}_i G^R_{\boldsymbol{k}}(\mathcal{E})v_j G^R_{\boldsymbol{k}}(\mathcal{E}-\hbar\omega)v_k G^A_{\boldsymbol{k}}(\mathcal{E})\\ +&f(\mathcal{E})\mathcal{T}_i G^\mathrm{R}_{\boldsymbol{k}}(\mathcal{E})v_k G^\mathrm{R}_{\boldsymbol{k}}(\mathcal{E}+\hbar\omega)v_j G^\mathrm{R}_{\boldsymbol{k}}(\mathcal{E})\\ -&f(\mathcal{E})\mathcal{T}_i G^\mathrm{R}_{\boldsymbol{k}}(\mathcal{E})v_k G^\mathrm{R}_{\boldsymbol{k}}(\mathcal{E}+\hbar\omega)v_j G^\mathrm{A}_{\boldsymbol{k}}(\mathcal{E})\\ +&f(\mathcal{E}-\hbar\omega)\mathcal{T}_i G^R_{\boldsymbol{k}}(\mathcal{E})v_j G^R_{\boldsymbol{k}}(\mathcal{E}-\hbar\omega)v_k G^A_{\boldsymbol{k}}(\mathcal{E})\\ +&f(\mathcal{E}+\hbar\omega)\mathcal{T}_i G^\mathrm{R}_{\boldsymbol{k}}(\mathcal{E})v_k G^\mathrm{R}_{\boldsymbol{k}}(\mathcal{E}+\hbar\omega)v_j G^\mathrm{A}_{\boldsymbol{k}}(\mathcal{E})\big],\end{aligned} \tag{10}$$

where $\mathcal{N}$ is the number of $\boldsymbol{k}$ points used to sample the Brillouin zone, $f(\mathcal{E})$ is the Fermi distribution function, $G^\mathrm{R}_{\boldsymbol{k}}(\mathcal{E})$ is the retarded Green's function, and $G^\mathrm{A}_{\boldsymbol{k}}(\mathcal{E}) = [G^\mathrm{R}_{\boldsymbol{k}}(\mathcal{E})]^\dagger$ is the advanced Green's function.

In collinear ferromagnets χ_{ijk} is zero when SOI is not included in the Hamiltonian. Formally, this can be deduced from Eq. (10) as follows: In the absence of SOI, both the Green's functions and the velocity operators can be chosen to be block-diagonal matrices with respect to the spin quantum number, such that neither the Green's functions nor the velocity operators mix spin-up and spin-down states. In contrast, matrix elements of the torque operator between spin-up states are zero, and also the matrix elements between spin-down states are zero; therefore, Eq. (10) evaluates to zero in the absence of SOI.

In order to simulate disorder and finite lifetimes of the electronic states we use the constant broadening Γ. Therefore, the energy dependence of the Green's function is known analytically:

$$G^\mathrm{R}_{\boldsymbol{k}}(\mathcal{E}) = \hbar\sum_n \frac{|\boldsymbol{k}n\rangle\langle\boldsymbol{k}n|}{\mathcal{E}-\mathcal{E}_{\boldsymbol{k}n}+i\Gamma}, \tag{11}$$

where $|\boldsymbol{k}n\rangle$ and $\mathcal{E}_{\boldsymbol{k}n}$ are eigenstates and eigenenergies, respectively, of the Hamiltonian in Eq. (1), i.e.,

$$H|\boldsymbol{k}n\rangle = \mathcal{E}_{\boldsymbol{k}n}|\boldsymbol{k}n\rangle. \tag{12}$$

This simple form of $G^\mathrm{R}_{\boldsymbol{k}}(\mathcal{E})$ allows us to perform the energy integrations in Eq. (10) analytically. The resulting expressions are given in Appendix B for the case of zero temperature. This constant broadening model of disorder is based purely on the electronic structure of the ordered system and neglects certain details of the scattering processes that are encoded in vertex correction terms and in the band-off-diagonal terms of the scattering self-energy. It models the band-diagonal terms of the scattering self-energy by the band-independent and $\boldsymbol{k}$-independent constant Γ. Therefore, it can be thought of as the "intrinsic" contribution, while mechanisms that depend on the detailed structure of the scatterers, which is encoded in vertex corrections and in the band-off-diagonal elements of the scattering self-energy, constitute the "extrinsic" contribution. When the scattering rate is small compared to the light frequency, which is typically the case for transition metals, extrinsic effects are expected to play a minor role.

The expressions that we use to evaluate the nonequilibrium spin density $\delta\boldsymbol{S}$, Eq. (5), are similar to Eqs. (9) and (10):

$$\delta S_i = -\frac{\hbar}{2}\frac{a_0^3 I}{c}\frac{\mathcal{E}_\mathrm{H}}{(\hbar\omega)^2}\mathrm{Im}\sum_{jk}\epsilon_j\epsilon_k^*\bar{\chi}_{ijk}, \tag{13}$$

where

$$\begin{aligned}\bar{\chi}_{ijk} = \frac{2}{\mathcal{N}\hbar a_0^2}\sum_{\boldsymbol{k}}\int d\mathcal{E}\\ \times \mathrm{Tr}\big[&f(\mathcal{E})\sigma_i G^\mathrm{R}_{\boldsymbol{k}}(\mathcal{E})v_j G^\mathrm{R}_{\boldsymbol{k}}(\mathcal{E}-\hbar\omega)v_k G^\mathrm{R}_{\boldsymbol{k}}(\mathcal{E})\\ -&f(\mathcal{E})\sigma_i G^R_{\boldsymbol{k}}(\mathcal{E})v_j G^R_{\boldsymbol{k}}(\mathcal{E}-\hbar\omega)v_k G^A_{\boldsymbol{k}}(\mathcal{E})\\ +&f(\mathcal{E})\sigma_i G^\mathrm{R}_{\boldsymbol{k}}(\mathcal{E})v_k G^\mathrm{R}_{\boldsymbol{k}}(\mathcal{E}+\hbar\omega)v_j G^\mathrm{R}_{\boldsymbol{k}}(\mathcal{E})\\ -&f(\mathcal{E})\sigma_i G^\mathrm{R}_{\boldsymbol{k}}(\mathcal{E})v_k G^\mathrm{R}_{\boldsymbol{k}}(\mathcal{E}+\hbar\omega)v_j G^\mathrm{A}_{\boldsymbol{k}}(\mathcal{E})\\ +&f(\mathcal{E}-\hbar\omega)\sigma_i G^R_{\boldsymbol{k}}(\mathcal{E})v_j G^R_{\boldsymbol{k}}(\mathcal{E}-\hbar\omega)v_k G^A_{\boldsymbol{k}}(\mathcal{E})\\ +&f(\mathcal{E}+\hbar\omega)\sigma_i G^\mathrm{R}_{\boldsymbol{k}}(\mathcal{E})v_k G^\mathrm{R}_{\boldsymbol{k}}(\mathcal{E}+\hbar\omega)v_j G^\mathrm{A}_{\boldsymbol{k}}(\mathcal{E})\big].\end{aligned} \tag{14}$$

In collinear ferromagnets $\bar{\chi}_{ijk}$ is zero when SOI is not included in the Hamiltonian. In the case of the spin components perpendicular to the magnetization the arguments by which this can be derived from Eq. (14) are the same as those in the case of χ_{ijk} discussed above: In the absence of SOI, Green's functions and velocity operators can be chosen such that they do not mix spin-up and spin-down states, while the matrix elements of the perpendicular component of the spin operator are zero between spin-up states and also between spin-down states. The induced spin parallel to the magnetization arises from the change of the difference between the number of spin-up electrons and the number of spin-down electrons. However, in the absence of SOI, the number operator of spin-up electrons commutes with the perturbation δH, and likewise, the number operator of spin-down electrons commutes with δH. Therefore, also the spin induced parallel to the magnetization is zero in collinear ferromagnets when SOI is not included in the Hamiltonian.

Equations (10) and (14) hold for continuous laser beams. Ultrashort laser pulses of 50-fs duration and light wavelength of 800 nm correspond to roughly 20 oscillations of the electric field vector. Therefore, the above formalism needs to be extended to describe time-dependent rather than stationary response functions in order to provide precise predictions of experiments with ultrashort laser pulses. However, for the discussion of torques and nonequilibrium spin polarization induced by 50-fs laser pulses, results obtained for continuous laser beams can serve as a useful estimate.

III. RESULTS

A. Computational details

We employ the full-potential linearized augmented-plane-wave (FLAPW) program FLEUR [29] in order to determine the electronic structure of bcc Fe, $L1_0$ FePt, and hcp Co self-consistently within the generalized gradient approximation [30] to density functional theory. The experimental lattice constants are used. In the case of Fe and FePt the crystallographic c and a axes are aligned with the z and y directions, respectively (Fig. 1 illustrates the coordinate frame). In the case of Co we performed two calculations in order to assess the anisotropy of the laser-induced torques: one calculation where the c axis is aligned with the z direction and one where the c axis is aligned with the x direction (in both calculations the a axis is in the y direction).

In order to perform the Brillouin zone integrations in Eqs. (10) and (14) computationally efficiently based on the Wannier interpolation technique [31], we constructed 18 maximally localized Wannier functions (MLWFs) per transition-metal atom from an $8 \times 8 \times 8$ $\boldsymbol{k}$ mesh [32,33]. In order to describe room-temperature experiments in Fe, FePt, and Co, it is a very good approximation to set the temperature in the Fermi distribution function $f(\mathcal{E})$ in Eqs. (10) and (14) to zero. Effects of room-temperature phonon scattering can be modeled by the phenomenological broadening parameter Γ in Eq. (11). The energy integrations in Eqs. (10) and (14) are performed analytically, as described in Appendix B. We vary Γ in the range from 5 meV to 0.4 eV. For this range of broadening Γ we find that not more than $256 \times 256 \times 256$ $\boldsymbol{k}$ points are needed in order to converge the Brillouin zone sampling in Eqs. (10) and (14).

B. Laser-induced torques

We discuss laser-induced torques for the laser intensity $I = 10\ \mathrm{GW/cm^2}$. The photon energy is set to 1.55 eV. The light is propagating into the x direction (as illustrated in Fig. 1), and the polarization vector is $\boldsymbol{\epsilon}_\lambda = (0,1,i\lambda)/\sqrt{2}$, where $\lambda = +1$ and $\lambda = -1$ describe left- and right-circularly polarized light, respectively. The magnetization is set along the z direction.

It is convenient to discuss the laser-induced torque $\boldsymbol{T}$ in terms of the equivalent effective magnetic field $\boldsymbol{B}^{\mathrm{eff}}$ that one needs to apply in order to produce the same torque on the magnetization. It is given by

$$\boldsymbol{B}^{\mathrm{eff}} = \frac{\boldsymbol{T} \times \hat{\boldsymbol{M}}}{\mu}, \tag{15}$$

where μ is the magnetic moment in the simulation volume. As illustrated in Fig. 1, an in-plane torque along the y direction corresponds to an effective magnetic field along the x direction, and an out-of-plane torque along the $-x$ direction corresponds to an effective magnetic field along the y direction. The effective field in the x direction B_x^{eff} arises due to the IFE in this case. The effective field in the y direction arises due to the OSTT.

Figure 2 shows the laser-induced effective magnetic fields in Fe, Co, and FePt. In the case of Co we show the results of two different calculations: one where the crystallographic c axis is in the z direction ($c\|z$) and one where it is in the x direction ($c\|x$). Both B_x^{eff} and B_y^{eff} are odd in helicity λ. The effective fields depend strongly on the broadening Γ, which varies between 5 meV and 0.4 eV in Fig. 2. In Fe B_y^{eff} is always larger than B_x^{eff} in the considered Γ range, while in FePt B_x^{eff} is always larger than B_y^{eff}. In Co B_x^{eff} dominates over B_y^{eff} for small and medium Γ, while for very large broadening B_y^{eff} becomes larger than B_x^{eff}. In Co the component B_x^{eff} exhibits a strong anisotropy at small Γ.

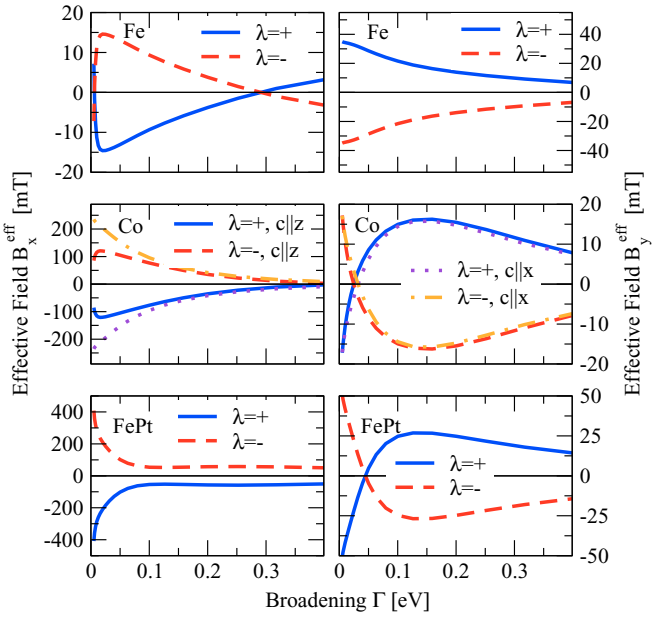

FIG. 2. Laser-induced effective magnetic fields B_x^{eff} (left column) and B_y^{eff} (right column) in Fe, Co, and FePt as a function of broadening Γ at $I = 10\ \mathrm{GW/cm^2}$. $\hat{\boldsymbol{M}}$ is in the z direction. $\lambda = +$ and $\lambda = -$ denote left- and right-circularly polarized light, respectively. In the case of Co, results are shown for the c axis in the z direction ($c\|z$) and the c axis in the x direction ($c\|x$).

In previous works we used $\Gamma = 25$ meV to model room-temperature experiments on Co/Pt bilayers [23]. At $\Gamma = 25$ meV we find $B_x^{\mathrm{eff}} = 118$ mT and $B_y^{\mathrm{eff}} = 0.23$ mT in Co for the $c\|z$ case. For $c\|x$ we find $B_x^{\mathrm{eff}} = 194$ mT and $B_y^{\mathrm{eff}} = 3.1$ mT in Co. Similarly, large anisotropies have been predicted for the anomalous Hall effect in Co [34]. At $\Gamma = 25$ meV the component B_x^{eff} strongly dominates over B_y^{eff}, leading to an initial in-plane tilt of the magnetization [see Fig. 1(a)], consistent with the experimental interpretation [14]. For a 50-fs laser pulse with a fluence of 1 $\mathrm{mJ/cm^2}$ [14], which corresponds to an intensity of the order of $I \approx 1\ \mathrm{mJ/cm^2}/(50\ \mathrm{fs}) = 20\ \mathrm{GW/cm^2}$, an effective field of 200 mT in Co was estimated from experiments [14], corresponding to roughly 100 mT at $I = 10\ \mathrm{GW/cm^2}$. The experimental geometry corresponds to the $c\|x$ case in our simulation. Our theoretical result of $B_x^{\mathrm{eff}} = 194$ mT is thus larger than the experimental estimate by roughly a factor of 2. One potential reason for the discrepancy is that laser pulses were used in the experiment, while our simulation assumes a continuous laser beam. Additionally, the effective magnetic field is strongly Γ dependent according to our calculation, and any disorder present in the 10-nm Co film used in the experiment might

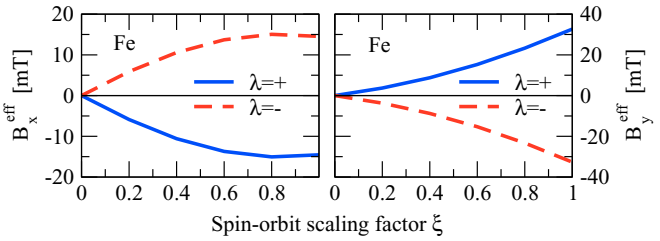

FIG. 3. Laser-induced effective magnetic fields B_x^{eff} (left) and B_y^{eff} (right) in Fe as a function of SOI scaling factor ξ at $I = 10\,\text{GW/cm}^2$. $\hat{\boldsymbol{M}}$ is in the z direction. $\lambda = +$ and $\lambda = -$ denote left- and right-circularly polarized light, respectively.

correspond to a value of Γ larger than 25 meV, which we assumed in this comparison.

At $\Gamma = 25$ meV, B_x^{eff} strongly dominates over B_y^{eff} in Co and FePt. On the other hand, the case of Fe shows that, generally, B_x^{eff} and B_y^{eff} can be of similar magnitude in transition-metal ferromagnets. If an Fe layer is used instead of the Co layer in Fig. 1, the initial magnetization tilt will be a mixture of in plane and out of plane according to our calculations. While the helicity-dependent component of the photocurrent in Co/Pt bilayers arises from an initial in-plane tilting [14] combined with the odd component of the ISOT, out-of-plane tilting also gives rise to photocurrents via the even ISOT component [15]. The photocurrent density $\boldsymbol{J}$ induced by the initial magnetization tilt in the bilayer geometry of Fig. 1 can be written as [14]

$$\boldsymbol{J} = -\frac{\gamma t^{\text{odd}}}{V}\hat{\boldsymbol{e}}_x \times [\hat{\boldsymbol{M}} \times \boldsymbol{B}^{\text{eff}}] - \frac{\gamma t^{\text{even}}}{V}\hat{\boldsymbol{e}}_x \times [\hat{\boldsymbol{M}} \times (\hat{\boldsymbol{M}} \times \boldsymbol{B}^{\text{eff}})], \tag{16}$$

where γ is the electron gyromagnetic factor, V is the volume, $\hat{\boldsymbol{e}}_x$ is a unit vector along the x axis, and the coefficients t^{odd} and t^{even} characterize the odd and even components of the SOT, respectively. When $\boldsymbol{B}^{\text{eff}}$ points in the x direction, the photocurrent is proportional to t^{odd}, and when $\boldsymbol{B}^{\text{eff}}$ points in the y direction, the photocurrent is proportional to t^{even}. In both cases the photocurrent is flowing along the magnetization direction. Therefore, we expect that the helicity-dependent component of the photocurrent in experiments analogous to the ones in Ref. [14] but based on Fe/Pt bilayers contains contributions from both the even and odd ISOTs. The differences in the effective fields $\boldsymbol{B}^{\text{eff}}$ between Fe, Co, and FePt suggest that ferromagnetic materials can be designed such that the IFE is zero and the OSTT is nonzero. Using such materials in experiments analogous to the ones in Ref. [14] would allow the contactless measurement of the even ISOT, which contains information about the spin Hall effect, from the helicity-odd component of the photocurrent. In fact, the helicity-even component of the photocurrent is already used for contactless measurement of the spin Hall effect [10].

In order to investigate the dependence of B_x^{eff} and B_y^{eff} on SOI, we linearly scale the spin-orbit interaction in the Hamiltonian with a factor ξ such that SOI is switched off for $\xi = 0$ and that the full SOI is active for $\xi = 1$. Figure 3 shows the laser-induced effective magnetic fields in Fe as a function of ξ. When SOI is switched off, B_x^{eff} and B_y^{eff} vanish, which proves that SOI is the origin of these laser-induced effective magnetic fields. The strong ξ dependence suggests using materials with large SOI in order to maximize the laser-induced torques. Indeed, among the ferromagnets considered in this study, FePt displays the largest values of B_x^{eff} and B_y^{eff}, which we attribute to the strong SOI of Pt.

C. Laser-induced spin polarization

We discuss the laser-induced spin polarization for the laser intensity $I = 10\,\text{GW/cm}^2$. The photon energy is set to 1.55 eV. The light is propagating into the x direction (as illustrated in Fig. 1), and the polarization vector is $\boldsymbol{\epsilon}_\lambda = (0, 1, i\lambda)/\sqrt{2}$, where $\lambda = +1$ and $\lambda = -1$ describe left- and right-circularly polarized light, respectively. The magnetization is set along the z direction.

We first discuss the two components of the laser-induced spin polarization $\delta\boldsymbol{S}$ that are perpendicular to the magnetization. These perpendicular components are expected to be related to B_x^{eff} and B_y^{eff} discussed in the previous section. Figure 4 shows that both δS_x and δS_y are odd in the helicity λ. Due to Eq. (6) we expect similarities between B_x^{eff} (Figure 2) and δS_x and between B_y^{eff} and δS_y. Indeed, in Fe δS_j exhibits the same qualitative dependence on Γ as its counterpart B_j^{eff} $(j = x, y)$. Since the electron spin magnetic moment is antiparallel to the electron spin, δS_j and B_j^{eff} are opposite in sign for a given helicity λ. In FePt only B_x^{eff} and δS_x behave similarly as a function of Γ, while B_y^{eff} and δS_y exhibit different trends, notably a sign change in B_y^{eff} that is absent in δS_y. In Co both δS_x and δS_y are strongly anisotropic for small Γ,

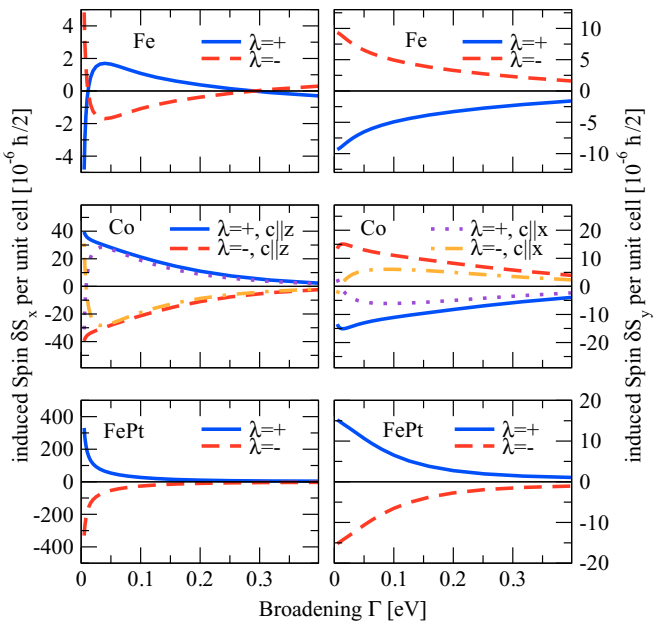

FIG. 4. Laser-induced spin polarization δS_x (left column) and δS_y (right column) in Fe, Co, and FePt as a function of broadening Γ at $I = 10\,\text{GW/cm}^2$. $\hat{\boldsymbol{M}}$ is in the z direction. $\lambda = +$ and $\lambda = -$ denote left- and right-circularly polarized light, respectively. In the case of Co, results are shown for the c axis in the z direction ($c \| z$) and the c axis in the x direction ($c \| x$).

while only B_x^{eff} displays strong anisotropy. These qualitative differences between δS_j and B_j^{eff} illustrate the importance of calculating the torques and effective magnetic fields from Eq. (6), which takes into account that the exchange field varies strongly on the atomic scale. On the other hand, in Fe, where δS_j and B_j^{eff} behave very similarly, it is tempting to define an effective exchange field $\Omega_{\text{eff}}^{\text{xc}}$ by the equation

$$\boldsymbol{T} = \frac{2\mu_{\text{B}}}{\hbar}\Omega_{\text{eff}}^{\text{xc}}\delta\boldsymbol{S}\times\hat{\boldsymbol{M}}. \tag{17}$$

The corresponding exchange splitting is

$$\Delta V_{\text{eff}} = 2\mu_{\text{B}}\Omega_{\text{eff}}^{\text{xc}} = -\frac{\hbar\mu B_j^{\text{eff}}}{\delta S_j}, \tag{18}$$

where μ is the magnetic moment per unit cell. From our results for B_j^{eff} and δS_j in Fe at $\Gamma = 25$ meV we obtain $\Delta V_{\text{eff}} = 2.6$ eV for $j = x$ and $\Delta V_{\text{eff}} = 1.1$ eV for $j = y$. The finding that we obtain different values for $j = x$ and $j = y$ shows that Eq. (17) cannot be used for precise calculations in Fe. However, since ΔV_{eff} has the expected order of magnitude of the exchange splitting in Fe, one can indeed use Eq. (17) for rough estimates of the torque $\boldsymbol{T}$ from the induced spin polarization $\delta\boldsymbol{S}$ in certain cases.

Next, we discuss the laser-induced spin polarization δS_z along the magnetization direction, which is shown in Fig. 5. We find δS_z to be almost helicity independent. Recent *ab initio* calculations for the case of the light-propagation direction parallel to the magnetization also find the laser-induced spin polarization along the magnetization direction to be almost helicity independent [16]. However, in contrast to Ref. [16] we consider the case of a light wave vector perpendicular to the magnetization (see Fig. 1) in our calculations. Thus, the laser-induced spin polarization parallel to the magnetization is almost helicity independent irrespective of whether the light wave vector is parallel or perpendicular to the magnetization in these metallic ferromagnets. Interestingly, δS_z reaches much larger values than the two perpendicular components δS_x and δS_y. For example, in FePt at $\Gamma = 25$ meV we find $\delta S_z = 1.2\times10^{-2}\hbar/2$ compared to only $\delta S_x = 9.2\times10^{-5}\hbar/2$ and $\delta S_y = 1.3\times10^{-5}\hbar/2$. In the case of Co δS_z depends on whether the c axis is in the x or z direction, but this anisotropy is less striking than for δS_x and δS_y at small Γ.

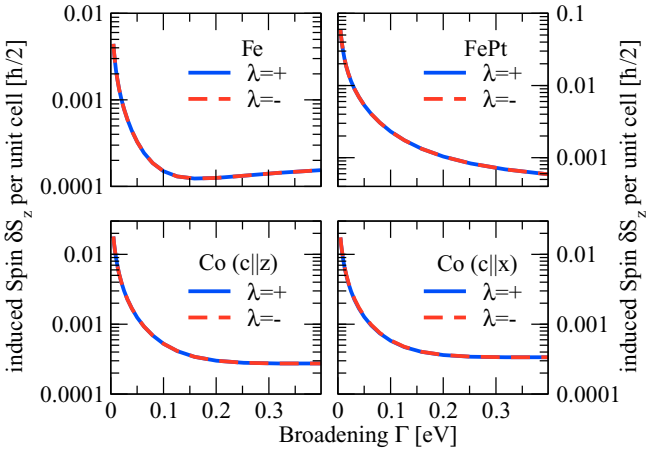

FIG. 5. Laser-induced spin polarization δS_z in Fe, Co, and FePt as a function of broadening Γ at $I = 10$ GW/cm^2. $\hat{\boldsymbol{M}}$ is in the z direction. $\lambda = +$ and $\lambda = -$ denote left- and right-circularly polarized light, respectively. In the case of Co, results are shown for the c axis in the z direction ($c\|z$) and the c axis in the x direction ($c\|x$).

IV. SUMMARY

We combine *ab initio* electronic structure calculations with the Keldysh nonequilibrium formalism in order to study laser-induced torques and nonequilibrium spin polarization in bcc Fe, hcp Co, and $L1_0$ FePt. Our calculations show that both IFE and OSTT are nonzero in these metallic ferromagnets. In the case of Fe the torques due to the OSTT are larger than those due to the IFE; in FePt the IFE dominates over the OSTT, and in Co the IFE is dominant only for small and medium quasiparticle broadenings. In view of this strong dependence of the IFE/OSTT ratio on the ferromagnetic material and the quasiparticle broadening (and hence the disorder in the system) it should be possible to design materials such that they display either IFE torques or OSTT but not both at the same time. This allows the contactless measurement of various spintronics effect in optical experiments. We find the torques and the perpendicular component of the nonequilibrium spin polarization to be odd in the helicity of the laser light, while the spin polarization that is induced parallel to the magnetization is helicity independent. This parallel component of the nonequilibrium spin polarization can be orders of magnitude larger than the perpendicular component. The comparison between laser-induced torques and laser-induced nonequilibrium spin density shows the importance of using the torque operator for calculations of laser-induced torques in realistic materials in order to capture the variation of the exchange field on the atomic scale. We find that both the laser-induced torques and the laser-induced nonequilibrium spin polarization are anisotropic in hcp Co. In the case of hcp Co we find good agreement between the calculated laser-induced torque and a recent experiment.

ACKNOWLEDGMENTS

We gratefully acknowledge computing time on the supercomputers of the Jülich Supercomputing Center and RWTH Aachen University as well as financial support from the program SPP 1538 Spin Caloric Transport of the Deutsche Forschungsgemeinschaft.

APPENDIX A: FORMALISM

The Green's function G in the presence of the perturbing laser field is obtained from the unperturbed Green's function G_{eq} via the Dyson equation on the Keldysh contour [35]

$$G(1,1') = G_{\text{eq}}(1,1') + \int d\,2\, G_{\text{eq}}(1,2)\frac{\delta H(2)}{\hbar}G(2,1'), \tag{A1}$$

where δH is the perturbation equation (2) due to the electric field of the laser. We iterate Eq. (A1) to obtain a power series in δH and identify the term quadratic in δH. Applying the Langreth theorem

$$(GGG)^{<} = G^{\text{R}}G^{\text{R}}G^{<} + G^{\text{R}}G^{<}G^{\text{A}} + G^{<}G^{\text{A}}G^{\text{A}} \tag{A2}$$

to the term quadratic in δH, we obtain

$$G_2^<(t,t') = \int dt_1 \int dt_2\, G_{\rm eq}^{\rm R}(t,t_1)\frac{\delta H(t_1)}{\hbar}G_{\rm eq}^{\rm R}(t_1,t_2)\frac{\delta H(t_2)}{\hbar}G_{\rm eq}^<(t_2,t') + \int dt_1 \int dt_2\, G_{\rm eq}^{\rm R}(t,t_1)\frac{\delta H(t_1)}{\hbar}G_{\rm eq}^<(t_1,t_2)\frac{\delta H(t_2)}{\hbar}G_{\rm eq}^{\rm A}(t_2,t') + \int dt_1 \int dt_2\, G_{\rm eq}^<(t,t_1)\frac{\delta H(t_1)}{\hbar}G_{\rm eq}^{\rm A}(t_1,t_2)\frac{\delta H(t_2)}{\hbar}G_{\rm eq}^{\rm A}(t_2,t'). \tag{A3}$$

Using

$$G_{\rm eq}^{\rm R}(t,t') = \frac{1}{2\pi\hbar}\int_{-\infty}^{\infty} d\mathcal{E}\, e^{-i\mathcal{E}(t-t')/\hbar}G_{\rm eq}^{\rm R}(\mathcal{E}) \tag{A4}$$

and

$$\int_{-\infty}^{\infty} dt_1 \int_{-\infty}^{\infty} dt_2\, e^{-\frac{i}{\hbar}\mathcal{E}(t-t_1)}e^{-i\omega_1 t_1}e^{-\frac{i}{\hbar}\mathcal{E}'(t_1-t_2)}e^{-i\omega_2 t_2}e^{-\frac{i}{\hbar}\mathcal{E}''(t_2-t')} = h^2\delta(\mathcal{E}-\hbar\omega_1-\mathcal{E}')\delta(\mathcal{E}'-\hbar\omega_2-\mathcal{E}'')e^{-\frac{i}{\hbar}\mathcal{E}t}e^{\frac{i}{\hbar}\mathcal{E}''t'}, \tag{A5}$$

the time integration of the product of three Green's functions can be performed easily:

$$\int dt_1 \int dt_2 G_{\rm eq}^{\alpha}(t,t_1)e^{-i\omega_1 t_1}G_{\rm eq}^{\alpha'}(t_1,t_2)e^{-i\omega_2 t_2}G_{\rm eq}^{\alpha''}(t_2,t) = \frac{e^{-i[\omega_1+\omega_2]t}}{h}\int d\mathcal{E}G_{\rm eq}^{\alpha}(\mathcal{E}+\hbar\omega_1)G_{\rm eq}^{\alpha'}(\mathcal{E})G_{\rm eq}^{\alpha''}(\mathcal{E}-\hbar\omega_2), \tag{A6}$$

where $\alpha,\alpha',\alpha'' = R, A, <$ and $\omega_1,\omega_2 = \pm\omega$. As discussed in Sec. II, we only need the dc component of $G_2^<$, which arises from all terms with $\omega_1 = -\omega_2 = \pm\omega$. It is given by

$$\begin{aligned} G_{\rm dc}^< = \frac{e^2E_0^2}{8\pi\omega^2\hbar^3}\int d\mathcal{E}\big\{&G_{\rm eq}^{\rm R}(\mathcal{E}-\hbar\omega)\boldsymbol{v}\cdot\boldsymbol{\epsilon}^*G_{\rm eq}^{\rm R}(\mathcal{E})\boldsymbol{v}\cdot\boldsymbol{\epsilon}G_{\rm eq}^<(\mathcal{E}-\hbar\omega) + G_{\rm eq}^{\rm R}(\mathcal{E}+\hbar\omega)\boldsymbol{v}\cdot\boldsymbol{\epsilon}G_{\rm eq}^{\rm R}(\mathcal{E})\boldsymbol{v}\cdot\boldsymbol{\epsilon}^*G_{\rm eq}^<(\mathcal{E}+\hbar\omega)\\ &+G_{\rm eq}^{\rm R}(\mathcal{E}-\hbar\omega)\boldsymbol{v}\cdot\boldsymbol{\epsilon}^*G_{\rm eq}^<(\mathcal{E})\boldsymbol{v}\cdot\boldsymbol{\epsilon}G_{\rm eq}^{\rm A}(\mathcal{E}-\hbar\omega) + G_{\rm eq}^{\rm R}(\mathcal{E}+\hbar\omega)\boldsymbol{v}\cdot\boldsymbol{\epsilon}G_{\rm eq}^<(\mathcal{E})\boldsymbol{v}\cdot\boldsymbol{\epsilon}^*G_{\rm eq}^{\rm A}(\mathcal{E}+\hbar\omega)\\ &+G_{\rm eq}^<(\mathcal{E}-\hbar\omega)\boldsymbol{v}\cdot\boldsymbol{\epsilon}^*G_{\rm eq}^{\rm A}(\mathcal{E})\boldsymbol{v}\cdot\boldsymbol{\epsilon}G_{\rm eq}^{\rm A}(\mathcal{E}-\hbar\omega) + G_{\rm eq}^<(\mathcal{E}+\hbar\omega)\boldsymbol{v}\cdot\boldsymbol{\epsilon}G_{\rm eq}^{\rm A}(\mathcal{E})\boldsymbol{v}\cdot\boldsymbol{\epsilon}^*G_{\rm eq}^{\rm A}(\mathcal{E}+\hbar\omega)\big\}. \end{aligned} \tag{A7}$$

Substituting Eq. (A7) into Eq. (7) and using

$$G_{\rm eq}^<(\mathcal{E}) = f(\mathcal{E})\big[G_{\rm eq}^{\rm A}(\mathcal{E}) - G_{\rm eq}^{\rm R}(\mathcal{E})\big] \tag{A8}$$

yield

$$\begin{aligned} \boldsymbol{T} = \frac{ie^2E_0^2}{8\pi\omega^2\hbar^3}\int d\mathcal{E}\, f(\mathcal{E})\mathrm{Tr}\{&[\boldsymbol{\mathcal{T}}R\Lambda^\dagger R^+\Lambda A] - [\boldsymbol{\mathcal{T}}R\Lambda^\dagger R^+\Lambda R] + [\boldsymbol{\mathcal{T}}R\Lambda R^-\Lambda^\dagger A] - [\boldsymbol{\mathcal{T}}R\Lambda R^-\Lambda^\dagger R]\\ &+[\boldsymbol{\mathcal{T}}R^-\Lambda^\dagger A\Lambda A^-] - [\boldsymbol{\mathcal{T}}R^-\Lambda^\dagger R\Lambda A^-] + [\boldsymbol{\mathcal{T}}R^+\Lambda A\Lambda^\dagger A^+] - [\boldsymbol{\mathcal{T}}R^+\Lambda R\Lambda^\dagger A^+]\\ &+[\boldsymbol{\mathcal{T}}A\Lambda^\dagger A^+\Lambda A] - [\boldsymbol{\mathcal{T}}R\Lambda^\dagger A^+\Lambda A] + [\boldsymbol{\mathcal{T}}A\Lambda A^-\Lambda^\dagger A] - [\boldsymbol{\mathcal{T}}R\Lambda A^-\Lambda^\dagger A]\}, \end{aligned} \tag{A9}$$

where we introduced the abbreviations $\Lambda = \boldsymbol{v}\cdot\boldsymbol{\epsilon}$, $\Lambda^\dagger = [\boldsymbol{v}\cdot\boldsymbol{\epsilon}]^\dagger = \boldsymbol{v}\cdot\boldsymbol{\epsilon}^*$, $R = G_{\rm eq}^{\rm R}(\mathcal{E})$, $A = G_{\rm eq}^{\rm A}(\mathcal{E})$, $R^+ = G_{\rm eq}^{\rm R}(\mathcal{E}+\hbar\omega)$, $A^+ = G_{\rm eq}^{\rm A}(\mathcal{E}+\hbar\omega)$, $R^- = G_{\rm eq}^{\rm R}(\mathcal{E}-\hbar\omega)$, and $A^- = G_{\rm eq}^{\rm A}(\mathcal{E}-\hbar\omega)$. Terms that contain more than one A can be rewritten as complex conjugates of terms with more than one R:

$$\begin{aligned} \boldsymbol{T} = \frac{ie^2E_0^2}{8\pi\omega^2\hbar^3}\int d\mathcal{E}\, f(\mathcal{E})\mathrm{Tr}\{&[\boldsymbol{\mathcal{T}}R\Lambda^\dagger R^+\Lambda A] - [\boldsymbol{\mathcal{T}}R\Lambda^\dagger R^+\Lambda R] + [\boldsymbol{\mathcal{T}}R\Lambda R^-\Lambda^\dagger A] - [\boldsymbol{\mathcal{T}}R\Lambda R^-\Lambda^\dagger R]\\ &+[\boldsymbol{\mathcal{T}}R^-\Lambda^\dagger R\Lambda A^-]^* - [\boldsymbol{\mathcal{T}}R^-\Lambda^\dagger R\Lambda A^-] + [\boldsymbol{\mathcal{T}}R^+\Lambda R\Lambda^\dagger A^+]^* - [\boldsymbol{\mathcal{T}}R^+\Lambda R\Lambda^\dagger A^+]\\ &+[\boldsymbol{\mathcal{T}}R\Lambda^\dagger R^+\Lambda R]^* - [\boldsymbol{\mathcal{T}}R\Lambda^\dagger R^+\Lambda A]^* + [\boldsymbol{\mathcal{T}}R\Lambda R^-\Lambda^\dagger R]^* - [\boldsymbol{\mathcal{T}}R\Lambda R^-\Lambda^\dagger A]^*\}. \end{aligned} \tag{A10}$$

Using the imaginary part to simplify the expression and introducing a Brillouin zone average over $\mathcal{N}\boldsymbol{k}$ points, we finally obtain

$$\begin{aligned} \boldsymbol{T} &= \frac{|e|^2E_0^2}{4\pi\omega^2\hbar^3\mathcal{N}}\sum_{\boldsymbol{k}}\int d\mathcal{E}\mathrm{Im}\mathrm{Tr}\{f(\mathcal{E})[\boldsymbol{\mathcal{T}}R_{\boldsymbol{k}}\Lambda R_{\boldsymbol{k}}^-\Lambda^\dagger R_{\boldsymbol{k}} + \boldsymbol{\mathcal{T}}R_{\boldsymbol{k}}\Lambda^\dagger R_{\boldsymbol{k}}^+\Lambda R_{\boldsymbol{k}}]\\ &\quad+[f(\mathcal{E}-\hbar\omega)-f(\mathcal{E})][\boldsymbol{\mathcal{T}}R_{\boldsymbol{k}}\Lambda R_{\boldsymbol{k}}^-\Lambda^\dagger A_{\boldsymbol{k}}] + [f(\mathcal{E}+\hbar\omega)-f(\mathcal{E})][\boldsymbol{\mathcal{T}}R_{\boldsymbol{k}}\Lambda^\dagger R_{\boldsymbol{k}}^+\Lambda A_{\boldsymbol{k}}]\}\\ &= \frac{a_0^3 I}{c}\left(\frac{\mathcal{E}_{\rm H}}{\hbar\omega}\right)^2\mathrm{Im}\sum_{ijk}\hat{\boldsymbol{e}}_i(\hat{\boldsymbol{e}}_j\cdot\boldsymbol{\epsilon})(\hat{\boldsymbol{e}}_k\cdot\boldsymbol{\epsilon}^*)\chi_{ijk}, \end{aligned} \tag{A11}$$

where $\hat{\boldsymbol{e}}_1$, $\hat{\boldsymbol{e}}_2$, and $\hat{\boldsymbol{e}}_3$ are unit vectors along the x, y, and z axes, respectively. The coefficient $\chi_{ijk} = \chi_{ijk}^{(1)} + \chi_{ijk}^{(2)}$ is given by

$$\chi_{ijk}^{(1)} = \frac{2}{\mathcal{N}\hbar a_0^2\mathcal{E}_{\rm H}}\sum_{\boldsymbol{k}}\int d\mathcal{E}\mathrm{Tr}\{[f(\mathcal{E}-\hbar\omega)-f(\mathcal{E})][\mathcal{T}_i R_{\boldsymbol{k}} v_j R_{\boldsymbol{k}}^- v_k A_{\boldsymbol{k}}] + [f(\mathcal{E}+\hbar\omega)-f(\mathcal{E})][\mathcal{T}_i R_{\boldsymbol{k}} v_k R_{\boldsymbol{k}}^+ v_j A_{\boldsymbol{k}}]\} \tag{A12}$$

and

$$\chi^{(2)}_{ijk} = \frac{2}{\mathcal{N}\hbar a_0^2 \mathcal{E}_\mathrm{H}} \sum_{\boldsymbol{k}} \int d\mathcal{E}\, f(\mathcal{E}) \mathrm{Tr}[\mathcal{T}_i R_{\boldsymbol{k}} v_j R^-_{\boldsymbol{k}} v_k R_{\boldsymbol{k}} + \mathcal{T}_i R_{\boldsymbol{k}} v_k R^+_{\boldsymbol{k}} v_j R_{\boldsymbol{k}}]. \tag{A13}$$

APPENDIX B: EXPRESSIONS AT $T = 0$ K

In the present paper we use the constant broadening Γ in order to simulate disorder and finite lifetimes of the electronic states. Therefore, the energy dependence of the Green's function is known analytically:

$$R_{\boldsymbol{k}} = G^\mathrm{R}_{\boldsymbol{k}}(\mathcal{E}) = \hbar \sum_n \frac{|\boldsymbol{k}n\rangle\langle\boldsymbol{k}n|}{\mathcal{E} - \mathcal{E}_{\boldsymbol{k}n} + i\Gamma}. \tag{B1}$$

This simple form of $G^\mathrm{R}_{\boldsymbol{k}}(\mathcal{E})$ allows us to perform the energy integrations in Eqs. (A12) and (A13) analytically. We discuss only the zero-temperature limit and therefore replace the Fermi function by the Heaviside step function as $f(\mathcal{E}) = \theta(\mathcal{E}_\mathrm{F} - \mathcal{E})$, where $\mathcal{E}_\mathrm{F}$ is the Fermi energy. Thus, we need the following two integrals for the evaluation of Eqs. (A12) and (A13) in the zero-temperature limit:

$$I_1(\mathcal{E}_1,\mathcal{E}_2,\mathcal{E}_3,\mathcal{E}_4) = \int_{-\infty}^{\mathcal{E}_4} \frac{\mathcal{E}_\mathrm{H}^2\, d\mathcal{E}}{(\mathcal{E} - \mathcal{E}_1 + i\Gamma)(\mathcal{E} - \mathcal{E}_2 + i\Gamma)(\mathcal{E} - \mathcal{E}_3 + i\Gamma)} \tag{B2}$$

and

$$I_2(\mathcal{E}_1,\mathcal{E}_2,\mathcal{E}_3,\mathcal{E}_4) = \int_{-\infty}^{\mathcal{E}_4} \frac{\mathcal{E}_\mathrm{H}^2\, d\mathcal{E}}{(\mathcal{E} - \mathcal{E}_1 + i\Gamma)(\mathcal{E} - \mathcal{E}_2 + i\Gamma)(\mathcal{E} - \mathcal{E}_3 - i\Gamma)}. \tag{B3}$$

In terms of $I_1(\mathcal{E}_1,\mathcal{E}_2,\mathcal{E}_3,\mathcal{E}_4)$ and $I_2(\mathcal{E}_1,\mathcal{E}_2,\mathcal{E}_3,\mathcal{E}_4)$ the coefficients $\chi^{(1)}_{ijk}$ and $\chi^{(2)}_{ijk}$ can be expressed as follows:

$$\begin{aligned}\chi^{(1)}_{ijk} = \frac{2}{\mathcal{N}} \sum_{\boldsymbol{k}nmm'} \mathrm{Im}\big\{&[I_2(\mathcal{E}_{\boldsymbol{k}m},\mathcal{E}_{\boldsymbol{k}m'} + \hbar\omega,\mathcal{E}_{\boldsymbol{k}n},\mathcal{E}_\mathrm{F} + \hbar\omega) - I_2(\mathcal{E}_{\boldsymbol{k}m},\mathcal{E}_{\boldsymbol{k}m'} + \hbar\omega,\mathcal{E}_{\boldsymbol{k}n},\mathcal{E}_\mathrm{F})]\mathcal{M}^{nmm'}_{ijk} \\ &+ [I_2(\mathcal{E}_{\boldsymbol{k}m},\mathcal{E}_{\boldsymbol{k}m'} - \hbar\omega,\mathcal{E}_{\boldsymbol{k}n},\mathcal{E}_\mathrm{F} - \hbar\omega) - I_2(\mathcal{E}_{\boldsymbol{k}m},\mathcal{E}_{\boldsymbol{k}m'} - \hbar\omega,\mathcal{E}_{\boldsymbol{k}n},\mathcal{E}_\mathrm{F})]\mathcal{M}^{nmm'}_{ikj}\big\}\end{aligned} \tag{B4}$$

and

$$\chi^{(2)}_{ijk} = \frac{2}{\mathcal{N}} \sum_{\boldsymbol{k}nmm'} \mathrm{Im}\big\{I_1(\mathcal{E}_{\boldsymbol{k}m},\mathcal{E}_{\boldsymbol{k}m'} + \hbar\omega,\mathcal{E}_{\boldsymbol{k}n},\mathcal{E}_\mathrm{F})\mathcal{M}^{nmm'}_{ijk} + I_1(\mathcal{E}_{\boldsymbol{k}m},\mathcal{E}_{\boldsymbol{k}m'} - \hbar\omega,\mathcal{E}_{\boldsymbol{k}n},\mathcal{E}_\mathrm{F})\mathcal{M}^{nmm'}_{ikj}\big\}, \tag{B5}$$

where

$$\mathcal{M}^{nmm'}_{ijk} = \frac{\langle\boldsymbol{k}n|\mathcal{T}_i|\boldsymbol{k}m\rangle\langle\boldsymbol{k}m|v_j|\boldsymbol{k}m'\rangle\langle\boldsymbol{k}m'|v_k|\boldsymbol{k}n\rangle}{\mathcal{E}_\mathrm{H}\left[a_0\frac{\mathcal{E}_\mathrm{H}}{\hbar}\right]^2}. \tag{B6}$$

The integrations in Eqs. (B2) and (B3) can be performed analytically. In the general case of $\mathcal{E}_1 \neq \mathcal{E}_2 \neq \mathcal{E}_3 \neq \mathcal{E}_1$ we obtain

$$\begin{aligned}I_1(\mathcal{E}_1,\mathcal{E}_2,\mathcal{E}_3,\mathcal{E}_4) = &\frac{\mathcal{E}_\mathrm{H}^2}{2(\mathcal{E}_1 - \mathcal{E}_2)(\mathcal{E}_1 - \mathcal{E}_3)} \ln\left[1 + \frac{(\mathcal{E}_1 - \mathcal{E}_4)^2}{\Gamma^2}\right] + \frac{\mathcal{E}_\mathrm{H}^2}{2(\mathcal{E}_2 - \mathcal{E}_3)(\mathcal{E}_2 - \mathcal{E}_1)} \ln\left[1 + \frac{(\mathcal{E}_2 - \mathcal{E}_4)^2}{\Gamma^2}\right] \\ &+ \frac{\mathcal{E}_\mathrm{H}^2}{2(\mathcal{E}_3 - \mathcal{E}_1)(\mathcal{E}_3 - \mathcal{E}_2)} \ln\left[1 + \frac{(\mathcal{E}_3 - \mathcal{E}_4)^2}{\Gamma^2}\right] + \frac{\mathcal{E}_\mathrm{H}^2}{i(\mathcal{E}_1 - \mathcal{E}_2)(\mathcal{E}_1 - \mathcal{E}_3)} \arctan\frac{\mathcal{E}_4 - \mathcal{E}_1}{\Gamma} \\ &+ \frac{\mathcal{E}_\mathrm{H}^2}{i(\mathcal{E}_2 - \mathcal{E}_3)(\mathcal{E}_2 - \mathcal{E}_1)} \arctan\frac{\mathcal{E}_4 - \mathcal{E}_2}{\Gamma} + \frac{\mathcal{E}_\mathrm{H}^2}{i(\mathcal{E}_3 - \mathcal{E}_1)(\mathcal{E}_3 - \mathcal{E}_2)} \arctan\frac{\mathcal{E}_4 - \mathcal{E}_3}{\Gamma}\end{aligned} \tag{B7}$$

and

$$\begin{aligned}I_2(\mathcal{E}_1,\mathcal{E}_2,\mathcal{E}_3,\mathcal{E}_4) = &\frac{\mathcal{E}_\mathrm{H}^2}{2(\mathcal{E}_1 - \mathcal{E}_2)(\mathcal{E}_1 - \mathcal{E}_3 - 2i\Gamma)} \ln\left[1 + \frac{(\mathcal{E}_1 - \mathcal{E}_4)^2}{\Gamma^2}\right] + \frac{\mathcal{E}_\mathrm{H}^2}{2(\mathcal{E}_2 - \mathcal{E}_3 - 2i\Gamma)(\mathcal{E}_2 - \mathcal{E}_1)} \ln\left[1 + \frac{(\mathcal{E}_2 - \mathcal{E}_4)^2}{\Gamma^2}\right] \\ &+ \frac{\mathcal{E}_\mathrm{H}^2}{2(\mathcal{E}_3 - \mathcal{E}_1 + 2i\Gamma)(\mathcal{E}_3 - \mathcal{E}_2 + 2i\Gamma)} \ln\left[1 + \frac{(\mathcal{E}_3 - \mathcal{E}_4)^2}{\Gamma^2}\right] + \frac{i\mathcal{E}_\mathrm{H}^2}{(\mathcal{E}_1 - \mathcal{E}_2)(\mathcal{E}_3 - \mathcal{E}_1 + 2i\Gamma)} \\ &\times \left[\frac{\pi}{2} + \arctan\frac{\mathcal{E}_4 - \mathcal{E}_1}{\Gamma}\right] + \frac{i\mathcal{E}_\mathrm{H}^2}{(\mathcal{E}_3 - \mathcal{E}_2 + 2i\Gamma)(\mathcal{E}_2 - \mathcal{E}_1)}\left[\frac{\pi}{2} + \arctan\frac{\mathcal{E}_4 - \mathcal{E}_2}{\Gamma}\right] \\ &+ \frac{i\mathcal{E}_\mathrm{H}^2}{(\mathcal{E}_3 - \mathcal{E}_1 + 2i\Gamma)(\mathcal{E}_3 - \mathcal{E}_2 + 2i\Gamma)}\left[\frac{\pi}{2} + \arctan\frac{\mathcal{E}_4 - \mathcal{E}_3}{\Gamma}\right].\end{aligned} \tag{B8}$$

Due to the energy denominators in Eq. (B7), numerical difficulties can arise when $\mathcal{E}_1 \neq \mathcal{E}_2 \neq \mathcal{E}_3 \neq \mathcal{E}_1$ is not satisfied. Therefore, when $\mathcal{E}_1 = \mathcal{E}_2 \neq \mathcal{E}_3$ we use instead of Eq. (B7) the expression

$$I_1(\mathcal{E}_1,\mathcal{E}_1,\mathcal{E}_3,\mathcal{E}_4) = \frac{\mathcal{E}_{\mathrm{H}}^2}{2(\mathcal{E}_1-\mathcal{E}_3)^2}\ln\left[\frac{\Gamma^2+(\mathcal{E}_3-\mathcal{E}_4)^2}{\Gamma^2+(\mathcal{E}_1-\mathcal{E}_4)^2}\right] + \frac{\mathcal{E}_{\mathrm{H}}^2}{i(\mathcal{E}_1-\mathcal{E}_3)^2}\left[\arctan\frac{\mathcal{E}_4-\mathcal{E}_3}{\Gamma} - \arctan\frac{\mathcal{E}_4-\mathcal{E}_1}{\Gamma}\right] + \frac{\mathcal{E}_{\mathrm{H}}^2}{(\mathcal{E}_3-\mathcal{E}_1)(\mathcal{E}_4-\mathcal{E}_1+i\Gamma)}. \tag{B9}$$

Applying $I_1(\mathcal{E}_1,\mathcal{E}_1,\mathcal{E}_3,\mathcal{E}_4) = I_1(\mathcal{E}_1,\mathcal{E}_3,\mathcal{E}_1,\mathcal{E}_4) = I_1(\mathcal{E}_3,\mathcal{E}_1,\mathcal{E}_1,\mathcal{E}_4)$ to Eq. (B9), one readily obtains expressions for $I_1(\mathcal{E}_1,\mathcal{E}_2,\mathcal{E}_3,\mathcal{E}_4)$ that can be used in the special cases $\mathcal{E}_1 \neq \mathcal{E}_2 = \mathcal{E}_3$ and $\mathcal{E}_1 = \mathcal{E}_3 \neq \mathcal{E}_2$.

Similarly, when $\mathcal{E}_1 = \mathcal{E}_2$, we do not use Eq. (B8), but instead

$$I_2(\mathcal{E}_1,\mathcal{E}_1,\mathcal{E}_3,\mathcal{E}_4) = \frac{\mathcal{E}_{\mathrm{H}}^2}{2(\mathcal{E}_1-\mathcal{E}_3-2i\Gamma)^2}\ln\left[\frac{\Gamma^2+(\mathcal{E}_3-\mathcal{E}_4)^2}{\Gamma^2+(\mathcal{E}_1-\mathcal{E}_4)^2}\right] + \frac{i\ \mathcal{E}_{\mathrm{H}}^2}{(\mathcal{E}_1-\mathcal{E}_3-2i\Gamma)^2}\left[\frac{\pi}{2}+\arctan\frac{\mathcal{E}_4-\mathcal{E}_3}{\Gamma}\right] + \frac{i\ \mathcal{E}_{\mathrm{H}}^2}{(\mathcal{E}_1-\mathcal{E}_3-2i\Gamma)^2}\left[\frac{\pi}{2}+\arctan\frac{\mathcal{E}_4-\mathcal{E}_1}{\Gamma}\right] + \frac{\mathcal{E}_{\mathrm{H}}^2}{(\mathcal{E}_3-\mathcal{E}_1+2i\Gamma)(\mathcal{E}_4-\mathcal{E}_1+i\Gamma)}. \tag{B10}$$

In the special case $\mathcal{E}_1 = \mathcal{E}_2 = \mathcal{E}_3$ we use

$$I_1(\mathcal{E}_1,\mathcal{E}_1,\mathcal{E}_1,\mathcal{E}_4) = -\frac{\mathcal{E}_{\mathrm{H}}^2}{2(\mathcal{E}_4-\mathcal{E}_1+i\Gamma)^2}. \tag{B11}$$

[1] A. Kirilyuk, A. V. Kimel, and T. Rasing, Rev. Mod. Phys. **82**, 2731 (2010).

[2] A. V. Kimel, A. Kirilyuk, P. A. Usachev, R. V. Pisarev, A. M. Balbashov, and T. Rasing, Nature (London) **435**, 655 (2005).

[3] C.-H. Lambert, S. Mangin, B. S. D. C. S. Varaprasad, Y. K. Takahashi, M. Hehn, M. Cinchetti, G. Malinowski, K. Hono, Y. Fainman, M. Aeschlimann *et al.*, Science **345**, 1337 (2014).

[4] R. John, M. Berritta, D. Hinzke, C. Müller, T. Santos, H. Ulrichs, P. Nieves, J. Walowski, R. Mondal, O. Chubykalo-Fesenko *et al.*, arXiv:1606.08723.

[5] P. Nemec, E. Rozkotova, N. Tesarova, F. Trojanek, E. De Ranieri, K. Olejnik, J. Zemen, V. Novak, M. Cukr, P. Maly *et al.*, Nat. Phys. **8**, 411 (2012).

[6] M. van Kampen, C. Jozsa, J. T. Kohlhepp, P. LeClair, L. Lagae, W. J. M. de Jonge, and B. Koopmans, Phys. Rev. Lett. **88**, 227201 (2002).

[7] M. Battiato, K. Carva, and P. M. Oppeneer, Phys. Rev. Lett. **105**, 027203 (2010).

[8] G. Malinowski, F. Dalla Longa, J. H. H. Rietjens, P. V. Paluskar, R. Huijink, H. J. M. Swagten, and B. Koopmans, Nat. Phys. **4**, 855 (2008).

[9] A. Melnikov, I. Razdolski, T. O. Wehling, E. T. Papaioannou, V. Roddatis, P. Fumagalli, O. Aktsipetrov, A. I. Lichtenstein, and U. Bovensiepen, Phys. Rev. Lett. **107**, 076601 (2011).

[10] T. Seifert, S. Jaiswal, U. Martens, J. Hannegan, L. Braun, P. Maldonado, F. Freimuth, A. Kronenberg, J. Henrizi, I. Radu *et al.*, Nat. Photonics **10**, 483 (2016).

[11] A. J. Schellekens, K. C. Kuiper, R. R. J. C. de Wit, and B. Koopmans, Nat. Commun. **5**, 4333 (2014).

[12] G.-M. Choi, C.-H. Moon, B.-C. Min, K.-J. Lee, and D. G. Cahill, Nat. Phys. **11**, 576 (2015).

[13] G.-M. Choi, Ph.D. thesis, University of Illinois at Urbana-Champaign, 2015.

[14] T. J. Huisman, R. V. Mikhaylovskiy, J. D. Costa, F. Freimuth, E. Paz, J. Ventura, P. P. Freitas, S. Blügel, Y. Mokrousov, T. Rasing *et al.*, Nat. Nanotechnol. **11**, 455 (2016).

[15] F. Freimuth, S. Blügel, and Y. Mokrousov, Phys. Rev. B **92**, 064415 (2015).

[16] M. Berritta, R. Mondal, K. Carva, and P. M. Oppeneer, Phys. Rev. Lett. **117**, 137203 (2016).

[17] A. Qaiumzadeh and M. Titov, Phys. Rev. B **94**, 014425 (2016).

[18] T. Misawa, T. Yokoyama, and S. Murakami, Phys. Rev. B **84**, 165407 (2011).

[19] K. Taguchi and G. Tatara, Phys. Rev. B **84**, 174433 (2011).

[20] K. Taguchi, J.-i. Ohe, and G. Tatara, Phys. Rev. Lett. **109**, 127204 (2012).

[21] P. M. Haney, D. Waldron, R. A. Duine, A. S. Nunez, H. Guo, and A. H. MacDonald, Phys. Rev. B **76**, 024404 (2007).

[22] P. M. Haney, R. A. Duine, A. S. Nunez, and A. H. MacDonald, J. Magn. Magn. Mater. **320**, 1300 (2008).

[23] F. Freimuth, S. Blügel, and Y. Mokrousov, Phys. Rev. B **90**, 174423 (2014).

[24] P. M. Haney, H.-W. Lee, K.-J. Lee, A. Manchon, and M. D. Stiles, Phys. Rev. B **88**, 214417 (2013).

[25] I. Turek, J. Kudrnovský, and V. Drchal, Phys. Rev. B **92**, 214407 (2015).

[26] S. Wimmer, K. Chadova, M. Seemann, D. Ködderitzsch, and H. Ebert, Phys. Rev. B **94**, 054415 (2016).

[27] K. Garello, I. M. Miron, C. O. Avci, F. Freimuth, Y. Mokrousov, S. Blügel, S. Auffret, O. Boulle, G. Gaudin, and P. Gambardella, Nat. Nanotechnol. **8**, 587 (2013).

[28] C. Ciccarelli, L. Anderson, V. Tshitoyan, A. J. Ferguson, F. Gerhard, C. Gould, L. W. Molenkamp, J. Gayles, J. Zelezny, L. Smejkal *et al.*, Nat. Phys. **12**, 855 (2016).

[29] FLEUR, http://www.flapw.de.

[30] J. P. Perdew, K. Burke, and M. Ernzerhof, Phys. Rev. Lett. **77**, 3865 (1996).
[31] N. Marzari, A. A. Mostofi, J. R. Yates, I. Souza, and D. Vanderbilt, Rev. Mod. Phys. **84**, 1419 (2012).
[32] A. A. Mostofi, J. R. Yates, Y.-S. Lee, I. Souza, D. Vanderbilt, and N. Marzari, Comput. Phys. Commun. **178**, 685 (2008).
[33] F. Freimuth, Y. Mokrousov, D. Wortmann, S. Heinze, and S. Blügel, Phys. Rev. B **78**, 035120 (2008).
[34] E. Roman, Y. Mokrousov, and I. Souza, Phys. Rev. Lett. **103**, 097203 (2009).
[35] J. Rammer and H. Smith, Rev. Mod. Phys. **58**, 323 (1986).